Dynamic energy flow analysis of the heat-electricity integrated energy systems with a novel decomposition-iteration algorithm

Shuai Yao[a], Wei Gu[a,*], Jianzhong Wu[b], Hai Lu[c], Suhan Zhang[a], Yue Zhou[b], Shuai Lu[a]

[a]*School of Electrical Engineering, Southeast University, Nanjing, 210096, China.*
[b]*School of Engineering, Cardiff University, Cardiff, CF24 3AA, UK.*
[c]*Yunnan Power Grid Co., Ltd, Kunming, 650217, China.*

Abstract

Simulation and operation optimization studies on the integrated energy system have received extensive attention recently for its potential in improving energy efficiency and increasing grid integration of renewable energy, where the task of energy flow calculation serves as a fundamental tool to determine the network states. This paper investigates the models and methods for dynamic energy flow analysis of two strongly coupled networks in the integrated energy systems — the power grid and the heating network. First, the complicated coupling mechanisms of power grid and heating network are thoroughly analyzed and classified into four representative coupling modes. On this basis, the detailed dynamic energy flow analysis method for each coupling mode is developed. Second, a refined difference scheme is applied to discretize the partial differential equations describing the long-lasting temperature dynamics in the heating network. The high-dimensional dicretized model is then solved by a novel decomposition-iteration algorithm. Compared with existing methods, this algorithm avoids deriving the gigantic coefficient matrix of network equations and can improve the accuracy of energy flow results. Finally, considering the systematical error caused by neglecting the inertial and adjusting constraints of heat sources, a revision stage is firstly introduced to correct the heat power output of the slack source and help obtain more accurate energy flow results. Case study shows that the proposed methods take 3.21s to obtain the dynamic energy flows of a coupled system consisting of a 118-node power grid and eight 35-node district heating networks over a 300-minutes simulation course, which is qualified to provide support for simulation and optimization related applications in practice.

Keywords:
Integrated energy systems, Heat and power, Dynamic energy flow, Timescale mismatch, Decomposition-iteration algorithm

1. Introduction

Recently, the wide application of integrated energy systems (IESs) [1–3] has endowed the studies on combined energy flow analysis of multi types of coupled energy networks with practical values. The basic task of energy flow calculation is to determine the network states with given operation conditions, including the power outputs at sources, the demands at loads and the network parameters.

In the IES, power grid (PG) and heating network (HN) are two widely-deployed energy supply networks. They are usually coupled through a group of facilities including cogeneration units (CUs), electric boilers (EBs) and heat pumps (HPs) [4, 5]. For one thing, joint operation of the heat and power subsystems can provide additional flexibility (e.g. the thermal inertia of HN and buildings) to enhance grid integration of renewable energy generations [6–8]; for another, strong correlation between two subsystems may cause cross-border propagation of disturbances and faults arising from either one of them [9, 10]. In view of this, combined energy flow analysis of PG and HN is needed to obtain the network states and to provide a basis for system monitoring and security analysis.

The concept of "energy flow" in IES is an extension of the "power flow" in power grid. In this paper, the task of combined energy flow analysis of PG and HN is to obtain: 1) the state variations of HN (including water temperatures, heat power flows and mass flow rates in each pipe) during the entire simulation course, and 2) a series of steady-state power flow points that describe the state variations of PG in this period (also known as the "time-series" power flows).

In general, the "quality-regulated" and "quantity-regulated" modes are two prevailing operation modes adopted in practical heating systems [11, 12]. The first mode is widely used in the primary heating network of centralized civil heating systems due to its stable hydraulic conditions. In this mode, mass flow rate in each pipe is predetermined and remains unchanged during operation while the temperatures of supply water at some heat sources are adjusted to satisfy the fluctuating heat loads. The second mode is typically applied in the secondary heating networks owing to its better regulating capacities. This paper focuses on the quality-regulated primary side of HN, which directly couples and interacts with the power grid.

To date, many studies on combined energy flow analysis of PG and HN have been carried out, with significant contributions achieved in model formulations and solution strategies, as summarized in Table 1. The time-series alternating current

*Corresponding author
Email address: wgu@seu.edu.cn (Wei Gu)

Table 1: A review of the studies on combined energy flow analysis of PG and HN.

Reference	Model of HN	Solution method	Convergence analysis	Node type defining of HN	Timescale match	Coupling analysis
[11]	TD-HL	Newton-Raphson technique (I & D)	×	✓	×	×
[13]	TD-HL	Newton algorithm (D)	×	×	×	✓
[14]	TD-HL	Gradient descent method (I)	×	×	×	×
[15]	TD-HL	Newton algorithm (I)	✓	×	×	×
[16]	TD-HL	Individual-based method (D)	×	×	✓	×
[17, 18]	TD-HL	Newton-Raphson technique (I)	×	✓	×	×
[19, 20]	TD-HL	Newton-Raphson technique (I)	×	×	×	×
[21]	TD-HL	Fixed-point based method (D)	✓	×	×	×
[22]	TD-HL	Newton algorithm (I)	✓	✓	×	×
[23]	TD-HL	Graph-based method (D)	×	×	×	×
[24]	TD-HL	Ring-to-radical reduction technique (D)	×	×	×	×
[25]	TD-HL	Industrial software integration (D)	×	×	×	×
[10]	PDE	Sequential simulation (D)	×	✓	×	×
[12]	PDE	Forward-backward iteration (D)	✓	✓	×	×
[27, 28]	redPDE	Fourier / Laplace transformation (D)	/	✓	×	×
This paper	PDE	"Decomposition-iteration" method (D)	✓	✓	✓	✓

(I) / (D): Solving the energy flow models of HN and PG in an *integrated* / *decoupled* way.

(AC) power flow model is widely used to approximate the dynamic state information of PG, while the adopted energy flow models of HN are generally divided into two categories: 1) the simplified algebraic model considering transmission delays and heat losses of HN [11, 13–26], denoted as TD-HL model; 2) the detailed model capturing the temperature transients in pipelines [10, 12, 27, 28], which is described by a group of partial differential equations (PDEs) derived from the law of energy conservation and can reveal more state information than the former one.

In this paper, a HN model that only considers the temperature dynamics and ignores the hydraulic transient process is classified as the "quasi-dynamic" model in order to distinguish it from the detailed simulation task that involves both thermal and hydraulic dynamics [10]. The node method model [29] is another quasi-dynamic HN model widely used in system optimal dispatch [30, 31]. It discretizes the water medium into small enough elements and computes the pipe outlet temperature with the history temperatures of all related elements. However, it omits the temperature wave propagation in the pipe and can cause temperature wave diffusion and smearing [32], enlarging the numerical errors in simulation or energy flow calculation. For this consideration, it is usually not adopted for combined energy flow analysis.

One major challenge of dynamic energy flow analysis of HE-IES lies in how to devise effective and efficient methods to solve the combined energy flow models, since the integration of PG and HN significantly enlarges the network scale and increases the solution complexity. For the energy flow model of PG, the Newton algorithm and its variant Newton-Raphson technique prove to be effective and are widely adopted, which are also employed in [11, 13, 15, 17–20, 22] to deal with the TD-HL HN model. The difference lies in that [11] and [13] take a decoupling strategy to solve the model of HN and PG separately in each round of iteration while the rest solve the two models in an integrated way.

Besides, several refined methods have also been proposed to solve the integrated energy flow models of PG and TD-HL HN, including the individual-based method [16], the fixed-point based method [21], the graph-based method [23], the ring-to-radical reduction technique [24] and the industrial software integration method [25], all of which are implemented under a similar decoupling solution framework as devised in [11] and [13] except the gradient descent iterative method developed in [14]. All of the above-mentioned methods report some edges over the traditional Newton's method.

Since the TD-HL HN model is a simplified approximation model, some studies have adopted the quasi-dynamic model described by PDEs, which is more accurate in capturing temperature dynamics yet more difficult to be integrated for combined energy flow analysis. Reference [12] employs the PDE HN model and proposes an iteration strategy for combined energy flow analysis, where the PDEs are discretized by the Forward Difference method and the energy flow model of HN is then solved with a forward-backward iteration method. However, for one thing, since the time steps for calculating the dynamic energy flows of HN and PG are different, timescale mismatch will appear when the HN and PG exchange information between one other in the decoupling solution framework. For another, the node types of coupling facilities determine the given conditions for each energy flow model and will thereby influence the overall decoupling solution strategy. Both of the above problems are neglected in [12], so it is with the work in [10] where the same HN model is adopted but a HN-PG sequential simulation method is developed for combined energy flow analysis.

The difference scheme derived from the Forward Difference method in [12] is simple and easy to implement, but with a relatively low convergence rate and should satisfy stringent stability and convergence conditions, which to some extent limits its applications. Moreover, the discretized energy flow model

after finite difference contains massive temporally and spatially correlated variables, making it difficult to be reformulated into a concise matrix representation of $\boldsymbol{Ax} = \boldsymbol{b}$. Traditional solution algorithms including the Jacobi and Gauss-Seidel methods [33] rely on the explicit form of coefficient matrix $\boldsymbol{A}$ to construct their iterative calculation schemes and cannot be employed here.

The above studies handle the HN model with finite difference method in time domain, while [27, 28, 34] tackle it from a different perspective — they apply the Fourier and Laplace transformations to convert the partial derivatives of time into algebraic terms and the PDEs are thereby transformed into ordinary differential equations. Combined energy flow analysis is then carried out in the domains of frequency and complex frequency. This method could achieve analytical solutions to temperature dynamics, if only the initial and boundary conditions of HN satisfy the Dirichlet Conditions and can be analytically expressed [27, 28]. However, such conditions can be hardly satisfied in some practical scenarios.

Besides, existing studies solve the network equations of HN to obtain the energy flows directly, in the meantime assuming the power outputs of heat sources can be adjusted to their set points as frequently and as quickly as needed. However, this is not the case in practice. Due to the physical inertial and maintenance costs of actuators like valves, the heat source will not change its power output over-frequently and it also has a ramp rate limit caused by the inertia of boilers and heat exchangers. If these adjusting constraints are left out, systematical errors will arise and the calculated energy flows will inevitably deviate from the real operation states.

By now the research gaps are concluded as: 1) the coupling mechanisms of PG and HN are still not clear. The problems that how the state variations of two subsystems mutually affect each other and how to settle the timescale mismatches occurred in the interactions between PG and HN are either neglected or incompletely discussed in previous studies; 2) the existing Forward Difference method employs a first-order numerical scheme with a relatively low convergence rate to solve the quasi-dynamic energy flow model of HN. Its generality is also limited due to strict stability and convergence requirements; 3) existing energy flow models fail to capture the adjusting characteristics of heat sources, which causes systematical errors that inevitably skew the energy flow results away from the real operation states. A more accurate model is desired to calculate closer-to-reality energy flows.

The motivations of this paper are to bridge the aforementioned gaps and to provide more generic and accurate tools for dynamic energy flow analysis of PG and HN. Main contributions of this paper are summarized as below.

1) The complicated coupling mechanisms of PG and HN were thoroughly analyzed and classified into four representative coupling modes. On this basis, the detailed dynamic energy flow analysis method for each coupling mode was developed, whereas previous studies either neglected or only covered one or two coupling modes.

2) A novel decomposition-iteration algorithm was developed to solve the high-dimensional quasi-dynamic energy flow model of HN after discretization. Compared with existing methods, this algorithm avoids deriving the gigantic coefficient matrix of network equations and can improve the stability and accuracy of energy flow results using a refined difference scheme.

3) The quasi-dynamic HN energy flow analysis method was further developed considering the ramp rate limits and the minimum adjustable interval constraints of heat sources, which considerably reduces the deviation between the calculated energy flows and the actual network states.

The remainder of this paper is organized as follows. The energy flow models of PG and HN are presented in Section 2. The interactions between PG and HN are discussed in Section 3, including a coupling analysis and a data processing method proposed to handle timescale mismatches. Section 4 expatiates the methods and algorithm for combined energy flow analysis, followed by a case study in Section 5. Lastly, the overall work of this paper and our future research focuses are concluded in Section 6 and 7.

2. Model Formulation

2.1. Energy Flow Models of HN and PG

The mathematical model for calculating the energy flows in HN is established based on the law of energy conservation [12, 35], as formulated in (1).

$$\begin{cases} \dfrac{\partial T_i}{\partial t} + v_i \dfrac{\partial T_i}{\partial x} + \dfrac{v_i}{\dot{m}_i c R_i}(T_i - T^{\mathrm{a}}) = 0 \quad \forall i \in \mathbb{E} \\ \sum_i (\dot{m}^{\mathrm{in}}_{n,i} \cdot T^{\mathrm{in}}_{n,i}) = T_n \cdot \sum_i \dot{m}^{\mathrm{in}}_{n,i} \quad \forall n \in \mathbb{V}^{\mathrm{i}},\, i \in \mathbb{E}^{\mathrm{in}}_n \\ T^{\mathrm{out}}_{n,j} = T_n \quad \forall n \in \mathbb{V}^{\mathrm{i}},\, j \in \mathbb{E}^{\mathrm{out}}_n \\ \phi_i = c \dot{m}_i (T^{\mathrm{s}}_i - T^{\mathrm{r}}_i) \quad \forall i \in \mathbb{E} \cup \mathbb{V} \end{cases} \tag{1}$$

where the first set of equations are PDEs describing how the water temperature in a pipe changes with time t and spatial coordinate x during transportation, i.e., the dynamic temperature propagation in each pipe. The second set describes when the water from multiple branches flows into a junction, what the temperature of the junction will be after flow mixing. The third set means that the water flows out of the same junction (into different branches) should have the same outflow temperature. The last set links the heat power with the supply and return water temperatures at each node.

In (1), T_i denotes the temperature of water in pipe i; T^{s} / T^{r} denotes the temperature of supply / return water; T^{a} is the ambient temperature outside the HN; v_i / $\dot{m}_i$ is the velocity / mass flow rate of water in pipe i; $\dot{m}^{\mathrm{in}}_{n,i}$ denotes the mass flow rate in the i^{th} pipe connected to node n and with water flowing into it; $T^{\mathrm{in}}_{n,i}$ / $T^{\mathrm{out}}_{n,j}$ denotes the temperature of water at the last / first spatial segment of the i^{th} / j^{th} pipe connected to node n and with water flowing into / out of it; ϕ_i is the injected or extracted heat power at node i or heat power flow in pipe i; and t / x is the independent variable of time / space domain. Parameters c and R_i denote the specific heat of water and the thermal resistance of pipe i. $\mathbb{E}$ / $\mathbb{V}$ / $\mathbb{V}^{\mathrm{i}}$ denotes the set of indices of all pipes / nodes / intermediate nodes in the HN; and $\mathbb{E}^{\mathrm{in}}_n$ / $\mathbb{E}^{\mathrm{out}}_n$ denotes the

set of indices of the pipes connected to node n and with water flowing into / out of it.

Mathematically, computing the energy flows of HN is solving (1) with a set of given conditions. These conditions include the system initial states and some information about the network parameters, topology, heat loads and sources. The consumed heat power at each load is an external disturbance to the HN — usually needs to be given (or predicted) beforehand, while the given information at heat sources needs to be determined based on their control modes.

Typically, the heat source is controlled under two independent modes based on whether it is involved in the task of heat regulation, i.e., whether it will adjust its heat power output to mitigate the system net power imbalance. If the heat source participates in the heat regulation, its power output will be adjusted to maintain the temperature of its supply water at the given values (usually follow the regulating curve of the climate compensator [36]), by means of increasing or decreasing the amount of steam extracted from turbines or boilers. If not, the heat power output will be preset and the temperature of supply water shall change with that of its return water.

To sum up, with the entire simulation process divided into a group of periods that constitute the set of $\mathbb{T}$, given conditions for calculating the quasi-dynamic energy flows in HN include:

1) Heat power output at each fixed-output source $\phi_{i,t}(i \in \mathbb{V}^{\text{s-f}}, t \in \mathbb{T})$.
2) Temperature of the supply water at each adjustable-output source $T^{\text{s}}_{i,t}(i \in \mathbb{V}^{\text{s-a}}, t \in \mathbb{T})$.
3) Mass flow rate in each pipe $\dot{m}_{i,t}(i \in \mathbb{E}, t \in \mathbb{T})$.
4) Heat power consumption at each load $\phi_{j,t}(j \in \mathbb{V}^{\text{l}}, t \in \mathbb{T})$.
5) Initial temperature distribution of the HN $T_{i,0}(i \in \mathbb{E})$.
6) Topological and physical parameters of the HN.

The task of energy flow analysis is solving (1) with the above known information to obtain the following outputs:

1) Temperature of the supply water at each fixed-output source $T^{\text{s}}_{i,t}(i \in \mathbb{V}^{\text{s-f}}, t \in \mathbb{T})$.
2) Heat power output at each adjustable-output source $\phi_{i,t}(i \in \mathbb{V}^{\text{s-a}}, t \in \mathbb{T})$.
3) Temperature distribution of both supply and return water networks $T_{i,t}(i \in \mathbb{E}, t \in \mathbb{T})$.

Compared with the slow dynamic process of heat and mass transfer in HN (typically lasting for hours), the dynamic processes in power grid (including the electromagnetic and electromechanical transients) are too short to be considered. Therefore, the time-series AC power flow model [37] is adopted to describe the quasi-dynamic state variations in PG. The active power balance equation should hold for all PV and PQ buses, while the reactive power balance equation should hold for all PQ buses, as formulated in (2) and (3).

$$P^{\text{bus}}_{i,t}(U,\theta) + P^{\text{d}}_{i,t} - P^{\text{g}}_{i,t} = 0 \quad \forall i \in \mathbb{I}^{\text{pv}} \cup \mathbb{I}^{\text{pq}}, t \in \mathbb{T} \tag{2}$$

$$Q^{\text{bus}}_{j,t}(U,\theta) + Q^{\text{d}}_{j,t} - Q^{\text{g}}_{j,t} = 0 \quad \forall j \in \mathbb{I}^{\text{pq}}, t \in \mathbb{T} \tag{3}$$

where P / Q denotes the active / reactive power; and U / θ denotes the voltage magnitude and angle phase. Superscript bus / d / g represents the power injections at bus / demand / generator; and pv / pq represents the PV / PQ bus.

2.2. Models of the Coupling Facilities

The PG and HN are interconnected via a group of coupling facilities including the back-pressure / extraction-condensing cogeneration units, electric boilers and heat pumps, the models of which are expressed in (4) – (7).

$$\phi^{\text{bp}}_t = P^{\text{bp}}_t \cdot \eta^{\text{bp}} \quad \forall t \in \mathbb{T} \tag{4}$$

$$Z_t = \frac{\phi^{\text{ec}}_t - \phi^{\text{ec}}_0}{P^{\text{ec}}_0 - P^{\text{ec}}_t} \quad \forall t \in \mathbb{T} \tag{5}$$

$$\phi^{\text{eb}}_t = P^{\text{eb}}_t \cdot \eta^{\text{eb}} \quad \forall t \in \mathbb{T} \tag{6}$$

$$\phi^{\text{hp}}_t = P^{\text{hp}}_t \cdot \text{COP}^{\text{hp}} \quad \forall t \in \mathbb{T} \tag{7}$$

where superscript bp / ec / eb / hp denotes the back-pressure unit / extraction-condensing unit / electric boiler / heat pump. Parameter η^{bp} / η^{eb} / COP^{hp} denotes the heat-to-power ratio / power-to-heat conversion efficiency / coefficient of performance; Z_t is the Z ratio quantifying the increased heat recovery and reduced electric power output of a cogeneration unit operated under the partially condensing scheme [38, 39]. ϕ^{ec}_0 / P^{ec}_0 denotes the heat / electric power output of the reference operating point.

2.3. Node Type Classification

In power flow calculation, buses in the power grid are classified as the PV, PQ and $V\theta$ types, based on the known information at each of them. Similarly, nodes in the heating network can also be classified into several types. Table 2 summarizes the node types of entities in both PG and HN.

Table 2: Node type classification in the PG and HN [12].

Entity	Category	Bus Type (PG)	Node Type (HN)
Generator	ES	$PV/PQ/V\theta$	/
TS	ES	$PV/PQ/V\theta$	/
Tie-line	ES	$PV/PQ/V\theta$	/
Wind Farm	ES	PV/PQ	/
PV Station	ES	PV/PQ	/
Electric Load	EL	PQ	/
Cogen. Unit	ES/HS	$PV/PQ/V\theta$	$mT^{\text{s}}/m\phi$
Heat Pump	EL/HS	PQ	$mT^{\text{s}}/m\phi$
Electric Boiler	EL/HS	PQ	$m\phi$
Coal/Gas Boiler	HS	/	$mT^{\text{s}}/m\phi$
Heat Load	HL	/	$m\phi$

Abbreviations — ES: Electric Source; TS: Transformer Substation; PV: Photo-Voltaic; EL: Electric Load; HS: Heat Source; HL: Heat Load.

In the HN, heat power output at the mT^{s} node can be adjusted to meet the fluctuating loads and mitigate system net heat power imbalance. In this sense, the mT^{s} node plays a similar role as the slack bus does in the PG, so it can be viewed as the "slack node" of the HN.

It is noteworthy that one type of bus or node might change to another when the operation constraints of these entities are violated. Case in point, the PV bus in the PG will change to the PQ one when the injected reactive power Q exceeds its limits ($Q < Q^{\min}$ or $Q > Q^{\max}$) — Q has to be fixed at its lower or upper bound. Similarly, in the HN, the heat source classified as

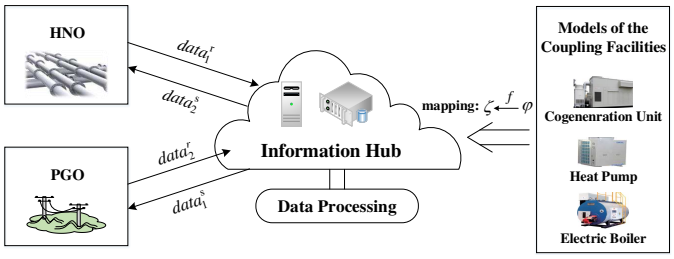

Figure 1: Diagram of how the information hub processes and exchanges data.

the mT^{s} node will change to the $m\phi$ one when more or less heat power than it could offer is required to maintain its temperatures of supply water at the set points.

3. Interactions Between the HN and PG

Basically, there are two ways for combined energy flow analysis: 1) combine the energy flow models of two subnetworks and solve them as a whole; 2) decouple the PG and HN at the coupling facilities and solve each model individually with some information exchanged between one another. The later avoids the challenge of solving large-scale heterogeneous network equations and is thereby adopted in this paper.

3.1. Matching Different Timescales

To ensure an efficient and privacy-preserving way of information exchange between the power grid operator (PGO) and the heating network operator (HNO), an independent entity called the information hub (IH) [21] is introduced. Main functions of the IH can be summarized as follows.

1) Process the received data to meet the timescale requirements of its receiver (HNO or PGO). Details of the data processing method will be presented in the follow-up.
2) Protect the privacy of each subnetwork through revealing only necessary state information to its counterpart. The exchanged information is determined by the coupling modes of PG and HN, which will be expatiated in Section 3.2.

In practical systems, the intervals for calculating the energy flows of PG and HN are usually different, causing timescale mismatches in the state information exchanged between PGO and HNO. To overcome this, a sampling method is proposed (and implemented by the IH) to process the received data before it is forwarded to its receiver. As is illustrated in Figure 1, the data received from the IH's sender is denoted as $data_1^{\mathrm{r}}$ (if received from the HNO) or $data_2^{\mathrm{r}}$ (if received from the PGO), which is a set of temporally discrete data points with a fixed interval τ^{r}, as formulated in (8).

$$data^{\mathrm{r}} = \{\varphi_t | \, t = n \cdot \tau^{\mathrm{r}}, \; n = 0, 1, 2, \cdots\} \tag{8}$$

where τ^{r} is the energy flow calculation interval of the IH's sender; and φ_t is the power injections at coupling facilities.

The first step to process the received data $\{\varphi_t\}$ from one subnetwork is to transform it into the state information (denoted as $\{\zeta_t\}$) of the other, based on the models of coupling facilities (see Section 2.2). For example, if $\{\varphi_t\}$ is the heat power output of a heat pump from the HNO, $\{\zeta_t\}$ would be its electric power input calculated through (7). The relationship between $\{\varphi_t\}$ and $\{\zeta_t\}$ are generally described by a mapping function f in (9).

$$mapping \; f: \; \{\varphi_t\} \rightarrow \{\zeta_t\}, \quad t = n \cdot \tau^{\mathrm{r}}, \; n = 0, 1, 2, \cdots \tag{9}$$

The second step is to transform the discrete data set $\{\zeta_t\}$ into a continuous staircase function $\zeta(t)$ through (10).

$$\zeta(t) = \zeta_{n\tau^{\mathrm{r}}}, \quad t \in [n\tau^{\mathrm{r}}, \; (n+1)\tau^{\mathrm{r}}), \; n = 0, 1, 2, \cdots \tag{10}$$

This step yields an intermediate data set for further processing:

$$data^{\mathrm{i}} = \{\zeta(t) | \, t \in [0, +\infty)\} \tag{11}$$

The last step is to get the desired data set (to be sent to the IH's receiver) through sampling on $data^{\mathrm{i}}$ at a regular time interval of τ^{s}, which is denoted as $data^{\mathrm{s}}$ in (12).

$$data^{\mathrm{s}} = \{\zeta(t) | \, t = n \cdot \tau^{\mathrm{s}}, \; n = 0, 1, 2, \cdots\} \tag{12}$$

where τ^{s} is the calculation interval of the IH's receiver.

The procedures of how the received $data^{\mathrm{r}}$ is transformed into $data^{\mathrm{i}}$, and then processed to $data^{\mathrm{s}}$ are illustrated by two examples in Figure 2, which correspond to the scenario of $\tau^{\mathrm{r}} \leq \tau^{\mathrm{s}}$ and $\tau^{\mathrm{r}} \geq \tau^{\mathrm{s}}$, respectively.

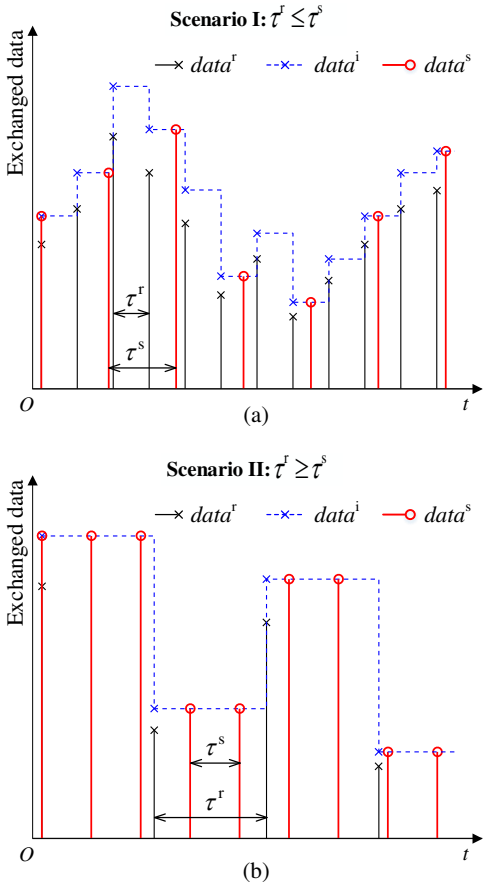

Figure 2: Diagram of how the information hub processes and exchanges data.

3.2. Coupling Modes of the PG and HN

Based on the node and bus types of the coupling facilities, four modes can be defined to describe the different coupling relationship between PG and HN:

- **Mode #1**: none of the cogeneration unit serves as the slack bus of PG, and none of the cogeneration unit or heat pump serves as the slack node of HN.
- **Mode #2**: none of the cogeneration unit serves as the slack bus of PG, and at least one cogeneration unit or heat pump serves as the slack node of HN.
- **Mode #3**: one cogeneration unit serves as the slack bus of PG, and none of the cogeneration unit or heat pump serves as the slack node of HN.
- **Mode #4**: one cogeneration unit serves as the slack bus of PG, and another cogeneration unit or heat pump serves as the slack node of HN.

In mode #1, since none of the coupling facilities serves as the slack node of HN or the slack bus of PG, the heat power outputs $\phi^{\mathrm{s}}_{i,t}$ and the active electric power inputs (or outputs) $P^{\mathrm{s}}_{i,t}$ of these coupling facilities are all given inputs to the energy flow models, as illustrated in Figure 3(a). This means the HN and PG are already decoupled — the HNO and PGO need not exchange any information for combined energy flow analysis, and the network states of the entire system can be obtained through solving each energy flow model separately.

In mode #2, coupling facilities do not serve as the slack bus of PG, so they will be the *PV* or *PQ* one. This means their active electric power inputs (or outputs) are given conditions to the energy flow model of PG. However, since one of the cogeneration unit or heat pump serves as the slack node of HN, its heat power output $\phi^{\mathrm{r}}_{i,t}$ needs to be first determined by solving the energy flow model of HN so that its coupled electric power output (or input) $P^{\mathrm{s}}_{i,t}$ could then be derived based on (4), (5) or (7), with which as a given input the energy flow model of PG could be subsequently solved. As depicted in Figure 3(b), the general procedures for combined energy flow analysis in this mode are: ① solve the energy flow model of HN to get the heat power output of the coupling facility that serves as the slack node; ② get the coupled active electric power output (or input) of this slack-node facility through its operation model; ③ solve the energy flow model of PG and output all the network states. The whole computing process is abbreviated as: HN → Coupling Facilities → PG.

The situation in mode #3 is just the opposite of that in mode #2. The active electric power output $P^{\mathrm{r}}_{i,t}$ of the cogeneration unit serving as the slack bus of PG needs to be first determined by solving the energy flow model of PG. On this basis, the heat power output $\phi^{\mathrm{s}}_{i,t}$ of this slack-bus facility could be derived through (4) or (5), with which the energy flow model of HN can be subsequently solved. As illustrated in Figure 3(c), the process of combined energy flow analysis in this mode can be abbreviated as: PG → Coupling Facilities → HN.

Things get more complicated in mode #4 where the slack node of HN and the slack bus of PG are two different coupling

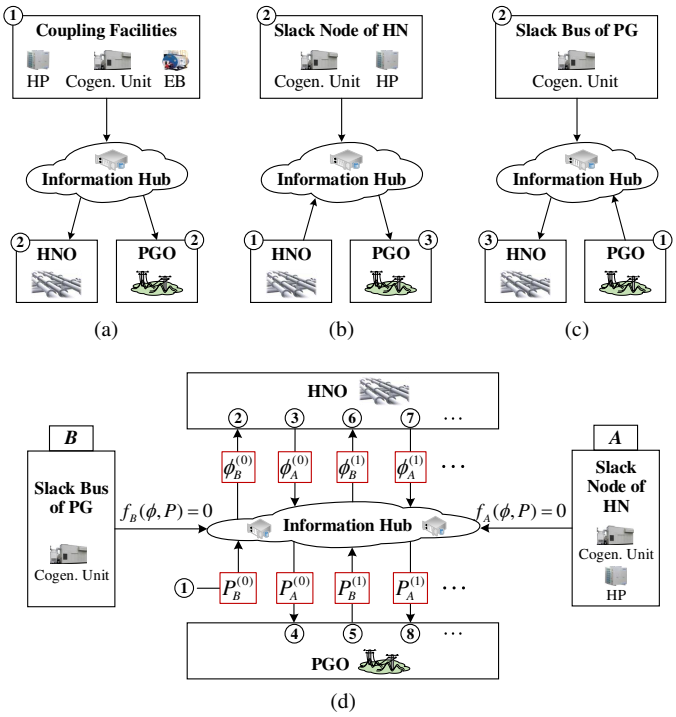

Figure 3: Interactions between the PG and HN in coupling mode #1 to #4. (a) Mode #1. (b) Mode #2. (c) Mode #3. (d) Mode #4.

facilities. In this mode, solving any one of the energy flow models requires part of the results of the other as given inputs. Both models of HN and PG cannot be solved separately or in sequence as presented in other modes. To tackle this problem, an iterative strategy is proposed. For the convenience of narration, let *A* and *B* denote the coupling facility serving as the slack node of HN and the slack bus of PG, respectively. As illustrated in Figure 3(d), the detailed procedures are: ① assume the initial value of P_B as $P_B^{(0)}$; ② get $\phi_B^{(0)}$ through the operation model of *B*, i.e. the equation presented in (4) or (5); ③ solve the energy flow model of HN to get the heat power output of the slack node $\phi_A^{(0)}$; ④ get $P_A^{(0)}$ through the operation model of *A*; ⑤ solve the energy flow model of PG to get the active electric power output of the slack bus $P_B^{(0)\prime}$. If $\left|P_B^{(0)\prime} - P_B^{(0)}\right|$ is less than the permitted error, terminate this iterative process and output the energy flow results; otherwise correct $P_B^{(1)}$ with the value of $P_B^{(0)\prime}$ and go to step ② to calculate $\phi_B^{(1)}$, $\phi_A^{(1)}$, $P_A^{(1)}$, and so forth. The whole process can be abbreviated as: Coupling Facility $B^{(0)}$ → $\mathrm{HN}^{(0)}$ → Coupling Facility $A^{(0)}$ → $\mathrm{PG}^{(0)}$ → Coupling Facility $B^{(1)}$ → $\mathrm{HN}^{(1)}$ → Coupling Facility $A^{(1)}$ → $\mathrm{PG}^{(1)}$ → $\cdots$.

It should be noted that in coupling mode #3 or #4, there is a cogeneration unit acting as the slack bus of PG. Since the heat and electric power outputs of a cogeneration unit are tightly correlated, its adjusting capacity as a slack-bus facility in PG can be highly influenced by its heat power output, posing tight limits on system operation. Therefore, coupling modes #3 or #4 are not recommended in practical systems.

4. Solution Method

4.1. Dealing With the PDEs

Mathematically, the energy flow model of HN in (1) is a hybrid system of PDEs and AEs. The basic solution strategy adopted here is to convert the part of PDEs (as presented in (13)) into AEs based on the finite difference method. By doing so, the energy flow model of HN can be transformed into a set of high-dimensional AEs, which is much easier to be solved in a standardized fashion.

$$\frac{\partial T_j}{\partial t} + v_j \frac{\partial T_j}{\partial x} + \frac{v_j (T_j - T^{\mathrm{a}})}{\dot{m}_j c R_j} = 0 \quad (j = 1, 2, \cdots, N^{\mathrm{p}}) \tag{13}$$

where j is the index of pipeline; N^{p} is the total number of pipelines, both the supply and return water pipelines included.

Let τ and h denote the temporal and spatial difference step size of each pipeline. For any pipeline $j (j \in \mathbb{E})$, substitute the temperature T_j and its partial derivatives in (13) with the following difference quotients [35, 40]:

$$\begin{cases} \dfrac{\partial T_j}{\partial t} = \dfrac{1}{2\tau}(T^{k+1}_{j,i-1} - T^{k}_{j,i-1} + T^{k+1}_{j,i} - T^{k}_{j,i}) + O(\tau^2) \\ \dfrac{\partial T_j}{\partial x} = \dfrac{1}{2h}(T^{k}_{j,i} - T^{k}_{j,i-1} + T^{k+1}_{j,i} - T^{k+1}_{j,i-1}) + O(h^2) \\ T_j = \dfrac{1}{4}(T^{k}_{j,i-1} + T^{k}_{j,i} + T^{k+1}_{j,i-1} + T^{k+1}_{j,i}) + O(h^2 + \tau^2) \end{cases} \tag{14}$$

where i and k denote the index of spatial and temporal difference layers, respectively. With some reorganization work we can get a specific difference scheme for approximating the numerical solutions of the PDEs:

$$\begin{aligned} &T^{k+1}_{j,i} = \varpi_{1,j} \cdot T^{k}_{j,i-1} + \varpi_{2,j} \cdot T^{k+1}_{j,i-1} + \varpi_{3,j} \cdot T^{k}_{j,i} + \varpi_{4,j} \cdot T^{\mathrm{a},k} \\ &(i = 1, 2, \cdots M_j;\ k = 0, 1, \cdots, N_j - 1;\ j = 1, 2, \cdots, N^{\mathrm{p}}) \end{aligned} \tag{15}$$

where M_j and N_j represent the number of the total discretized steps in space and time for the j^{th} pipeline; $\varpi_{1,j}$, $\varpi_{2,j}$, $\varpi_{3,j}$ and $\varpi_{4,j}$ are four parameters of the j^{th} pipeline that are defined for simplified representation, as formulated below:

$$\begin{aligned} \varpi_{1,j} &= \frac{1 + \frac{v_j\tau}{h} - \frac{v_j\tau}{2\dot{m}_j c R_j}}{1 + \frac{v_j\tau}{h} + \frac{v_j\tau}{2\dot{m}_j c R_j}}, & \varpi_{2,j} &= \frac{\frac{v_j\tau}{h} - 1 - \frac{v_j\tau}{2\dot{m}_j c R_j}}{1 + \frac{v_j\tau}{h} + \frac{v_j\tau}{2\dot{m}_j c R_j}} \\ \varpi_{3,j} &= \frac{1 - \frac{v_j\tau}{h} - \frac{v_j\tau}{2\dot{m}_j c R_j}}{1 + \frac{v_j\tau}{h} + \frac{v_j\tau}{2\dot{m}_j c R_j}}, & \varpi_{4,j} &= \frac{4 \times \frac{v_j\tau}{2\dot{m}_j c R_j}}{1 + \frac{v_j\tau}{h} + \frac{v_j\tau}{2\dot{m}_j c R_j}} \end{aligned} \tag{16}$$

Through the discretization in both space and time, the difference scheme in (15) can obtain the temperature dynamics in each pipeline layer by layer. As is shown in Figure 4, the temperature of water at the i^{th} space layer, $(k+1)^{\mathrm{th}}$ time layer can be calculated with a linear combination of the water temperatures at some other space and time layers (i.e. T^{k}_{i-1}, T^{k+1}_{i-1} and T^{k}_{i}), plus the ambient temperature at the k^{th} time layer $T^{\mathrm{a},k}$.

Here we have two more remarks on the difference scheme developed in (15). First, it is a system of AEs containing the number of $\sum_{j=1}^{N^{\mathrm{p}}} (M_j \cdot N_j)$ equations — its dimension could be terribly large if small h and τ are used, and solving it might require a considerable level of computing power and memory. Second, this scheme has a good performance in numerical calculation — it can always obtain the stable and convergent numerical results for any selected h and τ, i.e., unconditionally stable and convergent. Also, the computing error of it is well limited within the second order infinitesimals of the selected h and τ (i.e. $O(h^2 + \tau^2)$), which is lower than the node method model and the difference scheme developed by the Euler Formula in [12]. Detailed proof of these properties can be referred to from our previous work [35].

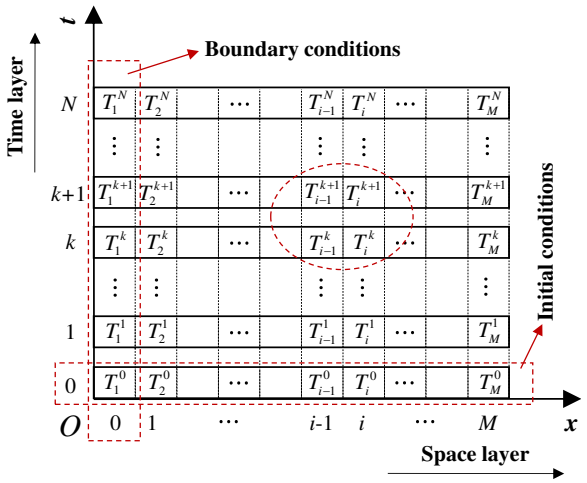

Figure 4: Computing process of the difference scheme listed in (15).

4.2. Selecting the calculating intervals for HN

The temporal interval τ for calculating the energy flow in the heating network generally depends on two factors: 1) the accuracy requirements of the energy flow analysis task; 2) the computation time limits that mainly affected by the network size, the overall simulation time, and the available computing resources. Choosing the interval τ is actually finding a trade-off between the two conflicting requirements mentioned above.

From a practical application point of view, we can start by choosing a commonly-used interval between 1 minute and 10 minutes. If the computation time limits are violated, try a larger interval until they are satisfied. Otherwise, try a smaller one until the computation time limits are violated. The selected temporal interval should be no smaller than this critical value.

As for the spatial interval h, it is recommended to be determined by (17) so as to avoid the dispersion and dissipation errors caused by finite difference [41].

$$h = v \cdot \tau \tag{17}$$

The selected spatial interval h can be different for each pipe. If the flow velocity v in each pipe does not differ much, a uniform spatial interval for all pipes is preferable as it can simplify the overall calculation process.

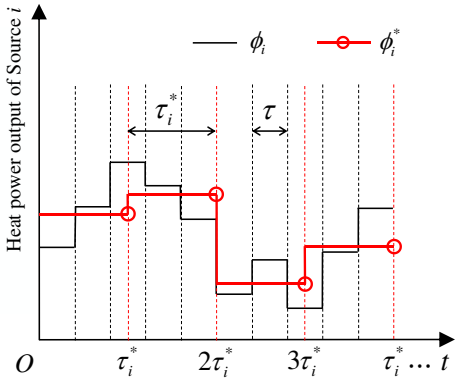

Figure 5: A comparison between the calculated ϕ_i and the updated ϕ_i^*.

4.3. Modifying the Energy Flow Results of HN

From Section 2.1, we know that the heat power output at each adjustable-output source $\phi_{i,t}(i \in \mathbb{V}^{\text{s-a}}, t \in \mathbb{T})$ can be obtained by solving (1). Since the temporal step size τ for calculating the water temperatures needs to be small enough (could be several tens of seconds) to ensure a low level of computing error, $\phi_{i,t}$ will accordingly change every tens of seconds as it is calculated with the same interval of τ in the finite difference method. Nevertheless, due to the physical constraints and maintenance costs of actuators like valves, the heat source cannot change its power output so frequently, and the inertial of boilers and heat exchangers would further impose a ramp rate limit for it. In this sense, the energy flow results obtained from Section 2.1 is actually the "ideal" operation states of HN, with a certain deviation from its actual states.

To characterize the adjusting constraints of heat sources, the ramp rate limit and the minimum adjustable interval of each source $\tau_{\min,i}(i \in \mathbb{V}^{\text{s}})$ are introduced, based on which, two main modifications are further implemented on the energy flow results obtained from Section 2.1, aiming to get closer-to-reality network states.

First, for each adjustable-output heat source, its heat power output ϕ_i should be reset as fixed ones (denoted as ϕ_i^*) within an adjustment interval. This ensures the actuators of each source to be adjusted only at some certain time points (named the scheduling time points). A sketch of the comparison between the calculated ϕ_i from Section 2.1 and the updated ϕ_i^* is illustrated in Figure 5, where τ_i^* represents the adjustment interval of this heat source ($\tau_i^* \geq \tau_{\min,i}$).

As discussed in Section 2.1, these adjustable-output sources are classified as the mT^{s} nodes in HN. This means the temperature of supply water at each one of them $T_i^{\text{s}}(i \in \mathbb{V}^{\text{s-a}})$ should be maintained at their set points, through the way of adjusting its heat power output ϕ_i. However, since ϕ_i cannot be adjusted as frequently as required, T_i^{s} cannot be kept as it should be. To reduce the deviation between T_i^{s} and their set points, the arithmetic average of the calculated ϕ_i from Section 2.1 within an adjustment interval τ_i^* is used as the updated fixed power output ϕ_i^*, as expressed in (18).

$$\phi_{ik}^* = \frac{1}{\tau_i^*} \int_{(k-1)\tau_i^*}^{k\tau_i^*} \phi_{ik}(t) \cdot dt \quad \forall k \in \mathbb{T}_i^{\text{adj}},\ i \in \mathbb{V}^{\text{s-a}} \tag{18}$$

where $\mathbb{T}_i^{\text{adj}}$ is the set of indices of all adjustment intervals.

At each scheduling time point, the power output of a heat source cannot increase or decrease too much compared with that at its former time point, as formulated below.

$$R^{\text{down}} \leq \phi_{i(k+1)}^* - \phi_{ik}^* \leq R^{\text{up}},\ \forall k, k+1 \in \mathbb{T}^{\text{adj}}, i \in \mathbb{V}^{\text{s-a}} \tag{19}$$

where R^{down} and R^{up} are the ramp down and up limits of a heat source, respectively. If the constraints in (19) are violated, $\phi_{i(k+1)}^*$ should be fixed at $\left(\phi_{ik}^* + R^{\text{down}}\right)$ or $\left(\phi_{ik}^* + R^{\text{up}}\right)$.

Second, once the heat power outputs of those adjustable-output sources are updated according to (18) and (19), the given information at them turns to be the mass flow rate $\dot{m}_{i,t}$ and the updated heat power output $\phi_{i,t}^*$. This means the node type of these sources changes from the mT^{s} node to the $m\phi$ one. Therefore, a revision stage is proposed to modify the preliminary energy flow results obtained from Section 2.1.

In this stage, the heat power outputs of all heat sources are fixed, and the given conditions for energy flow analysis are:

1) Heat power output at each source $\phi_{i,t}(i \in \mathbb{V}^{\text{s}}, t \in \mathbb{T})$.
2) Mass flow rate in each pipe $\dot{m}_{i,t}(i \in \mathbb{E}, t \in \mathbb{T})$.
3) Heat power consumption at each load $\phi_{j,t}(j \in \mathbb{V}^{\text{l}}, t \in \mathbb{T})$.
4) Initial temperature distribution of the HN $T_{i,0}(i \in \mathbb{E})$.
5) Topological and physical parameters of the HN.

The target in this stage is to obtain the temperature distribution of both supply and return water networks $T_{i,t}(i \in \mathbb{E}, t \in \mathbb{T})$ through re-solving the energy flow model of HN in (1).

4.4. The Decomposition-Iteration Algorithm

Overall, computing the energy flows in HN is formulated as a two-stage problem: in Stage I, (1) is solved to get the preliminary energy flows; in Stage II, the heat power output of each adjustable-output source $\phi_{j,t}$ obtained from Stage I is updated as $\phi_{j,t}^*$ through (18) and (19), and the energy flow model is resolved to get the final modified results. The "decomposition-iteration" algorithm is implemented in both stages.

The discretized energy flow model of HN is a system of massive linear AEs. Traditional methods including the Jacobi and Gauss-Seidel iterative strategies solve the linear AEs (with the standard form of $\boldsymbol{Ax} = \boldsymbol{b}$) by constructing a certain iterative calculation scheme $\boldsymbol{x}^{(k+1)} = \boldsymbol{Cx}^{(k)} + \boldsymbol{d}$. However, in practical HN, the dimension of variable vector $\boldsymbol{x}$ is super large after discretization and most of the variables are highly correlated in both space and time due to finite difference, which bring about great difficulty in obtaining the coefficient matrix $\boldsymbol{A}$ and reformulating the original model into the standard form of $\boldsymbol{Ax} = \boldsymbol{b}$. This means the aforementioned traditional methods that rely on the explicit expression of matrix $\boldsymbol{A}$ to construct their iterative calculation schemes do not apply here.

In view of this, we hope to develop a solution method that does not rely its iterative strategies on matrix $\boldsymbol{A}$. This idea inspires the formulation of the "decomposition-iteration" algorithm, which includes two basic steps.

Step 1: decompose the original problem of $\boldsymbol{Ax} = \boldsymbol{b}$ into several sub-problems expressed as below.

$$\begin{aligned} \boldsymbol{x}_{\boldsymbol{2}}^{(k)} &= \boldsymbol{C_1} \cdot \boldsymbol{x}_{\boldsymbol{1}}^{(k)} + \boldsymbol{d_1} \\ \boldsymbol{x}_{\boldsymbol{3}}^{(k)} &= \boldsymbol{C_2} \cdot \boldsymbol{x}_{\boldsymbol{2}}^{(k)} + \boldsymbol{d_2} \\ &\cdots \qquad\qquad , \ k = 0, 1, \cdots \\ \boldsymbol{x}_{\boldsymbol{n}}^{(k)} &= \boldsymbol{C_{n-1}} \cdot \boldsymbol{x}_{\boldsymbol{n-1}}^{(k)} + \boldsymbol{d_{n-1}} \\ \boldsymbol{x}_{\boldsymbol{1}}^{(k+1)} &= \boldsymbol{C_n} \cdot \boldsymbol{x}_{\boldsymbol{n}}^{(k)} + \boldsymbol{d_n} \end{aligned} \tag{20}$$

where $\boldsymbol{x_i}\,(i = 1, 2, \cdots, n)$ are the reconstructed variable vectors from $\boldsymbol{x}$; $\boldsymbol{C_1}$, $\boldsymbol{C_2}$, $\cdots$, $\boldsymbol{C_n}$ are constant coefficient matrices; $\boldsymbol{d_1}$, $\boldsymbol{d_2}$, $\cdots$, $\boldsymbol{d_n}$ are constant vectors; k denotes the index of each round of iterative calculation.

In this way, matrix $\boldsymbol{A}$ is broken up into a group of smaller scale coefficient matrices $\boldsymbol{C_i}\,(i = 1, 2, \cdots, n)$, and we no longer need the explicit form of $\boldsymbol{A}$ to solve the original problem.

Step 2: Assume the initial value of $\boldsymbol{x_1}$ to be $\boldsymbol{x}_{\boldsymbol{1}}^{(0)}$, and solve all the sub-problems in (20) iteratively until a convergent solution to $\boldsymbol{x_1}$ is obtained. The rest variables $\boldsymbol{x_i}\,(i = 2, 3, \cdots, n)$ and $\boldsymbol{x}$ can be further derived.

As we can see, one of the key points of this algorithm is to properly select the starting variable vector $\boldsymbol{x_1}$ to start the computing process. To the best, we hope the solution of $\boldsymbol{x_1}$ is easy to pre-estimate and can be used to compute $\boldsymbol{x_i}\,(i = 2, 3, \cdots, n)$ in the simplest way as possible. In the case of solving (1) specifically, the temperatures of supply water at all fixed-output sources $T_{j,t}^{\mathrm{s}}(j \in \mathbb{V}^{\text{s-f}}, t \in \mathbb{T})$ are selected to constitute $\boldsymbol{x_1}$ out of the following considerations: first, $T_{j,t}^{\mathrm{s}}$ will not deviate much from their design values when operated in the off-design conditions. In most cases, simply with these design values as an initial guess of $\boldsymbol{x_1}$, convergent results can be obtained; second, the process of computing $\boldsymbol{x_i}\,(i = 2, 3, \cdots, n)$ and updating $\boldsymbol{x_1}$ only involves simple operations on some small-scale matrices, as presented in Algorithm 1: computing $\boldsymbol{x}_{\boldsymbol{i}}^{(k)}\,(i = 2, 3, \cdots, n)$ corresponds to Step 4 to 6 and 15 to 17 in both stages while updating $\boldsymbol{x}_{\boldsymbol{1}}^{(k+1)}$ corresponds to Step 7 and 18. This means the workload in each round of iteration is moderate, which also facilitates the fast solution to the entire model.

The detailed procedures of the developed algorithm in solving the energy flow models of HN in both Stage I and II are presented in Algorithm 1. In each stage, the original energy flow model is divided into four sub-problems:

1) Compute the temperature distribution of supply water network using the supply water temperatures at heat sources.
2) Compute the return water temperatures at all load nodes using the consumed heat power and supply water temperatures at them.
3) Compute the temperature distribution of return water network using the return water temperatures at all load nodes.
4) Update the supply water temperatures at heat sources using the generated heat power and return water temperatures at them.

Algorithm 1: The "decomposition-iteration" method

1 *Initialization:* $t \in \mathbb{T}$, input $\phi_{i,t}(i \in \mathbb{V}^{\text{s-f}})$, $T_{i,t}^{\mathrm{s}}(i \in \mathbb{V}^{\text{s-a}})$, $\dot{m}_{i,t}(i \in \mathbb{E})$, $\phi_{j,t}(j \in \mathbb{V}^{\mathrm{l}})$, $T_{i,0}(i \in \mathbb{E})$ and network parameters.

*** **Stage I:** compute the preliminary energy flows in HN.

begin

2 Define the convergence tolerance err_1, the number of iterations $k = 0$, and the convergence marker $flag = 0$; make an initial guess of $T_{j,t}^{\mathrm{s}}$ as $T_{j,t}^{\mathrm{s}(0)}(j \in \mathbb{V}^{\text{s-f}})$.

3 **while** $flag = 0$ **do**

4 Compute the temperature distribution of supply water network $T_{j,t}^{\mathrm{s}(k)}(j \in \mathbb{E}^{\mathrm{s}})$ according to (A.1).

5 Compute the temperature of return water at each load $T_{j,t}^{\mathrm{r}(k)}(j \in \mathbb{V}^{\mathrm{l}})$ according to (A.2).

6 Compute the temperature distribution of return water network $T_{j,t}^{\mathrm{s}(k)}(j \in \mathbb{E}^{\mathrm{r}})$ according to (A.3).

7 Compute the updated values of the guessed varables $T_{j,t}^{\mathrm{s}(k)}$ as $T_{j,t}^{\mathrm{s}(k+1)}(j \in \mathbb{V}^{\text{s-f}})$ according to (A.4).

8 **if** $\max\limits_{j \in \mathbb{V}^{\text{s-f}}, t \in \mathbb{T}} \left| T_{j,t}^{\mathrm{s}(k+1)} - T_{j,t}^{\mathrm{s}(k)} \right| \le err_1$ **then**

9 $flag = 1$.

10 $k = k + 1$.

11 Output the preliminary energy flows: $T_{j,t}^{\mathrm{s}}(j \in \mathbb{V}^{\text{s-f}})$, $\phi_{j,t}(j \in \mathbb{V}^{\text{s-a}})$ and $T_{j,t}(j \in \mathbb{E})$.

*** **Stage II:** modify the preliminary energy flow results of HN.

begin

12 Update $\phi_{j,t}$ obtained from *Stage I* as $\phi_{j,t}^{*}(j \in \mathbb{V}^{\text{s-a}})$ according to (18) and (19).

13 Define the convergence tolerance err_2, the number of iterations $k = 0$, and the convergence marker $flag = 0$; make an initial guess of $T_{j,t}^{\mathrm{s}}$ as $T_{j,t}^{\mathrm{s}(0)}(j \in \mathbb{V}^{\mathrm{s}})$.

14 **while** $flag = 0$ **do**

15 Step 4.

16 Step 5.

17 Step 6.

18 Compute the updated values of the guessed varables $T_{j,t}^{\mathrm{s}(k)}$ as $T_{j,t}^{\mathrm{s}(k+1)}(j \in \mathbb{V}^{\mathrm{s}})$ according to (A.5).

19 **if** $\max\limits_{j \in \mathbb{V}^{\mathrm{s}}, t \in \mathbb{T}} \left| T_{j,t}^{\mathrm{s}(k+1)} - T_{j,t}^{\mathrm{s}(k)} \right| \le err_2$ **then**

20 $flag = 1$.

21 $k = k + 1$.

22 Output the modified energy flows: $T_{j,t}(j \in \mathbb{E})$.

By iteratively solving these sub-problems until the maximal difference between the two latest updated supply water temperatures decreases to within their convergence tolerances, we are able to get the final solutions to the original energy flow model.

Moreover, the convergence of this algorithm relies on the properties of coefficient matrices $\boldsymbol{C_i}\,(i = 1, 2, \cdots, n)$, which are directly influenced by the network topology, the parameters of pipes, and the difference step sizes. Detailed convergence analysis is presented in [42], where the necessary and sufficient convergence condition for this algorithm is given.

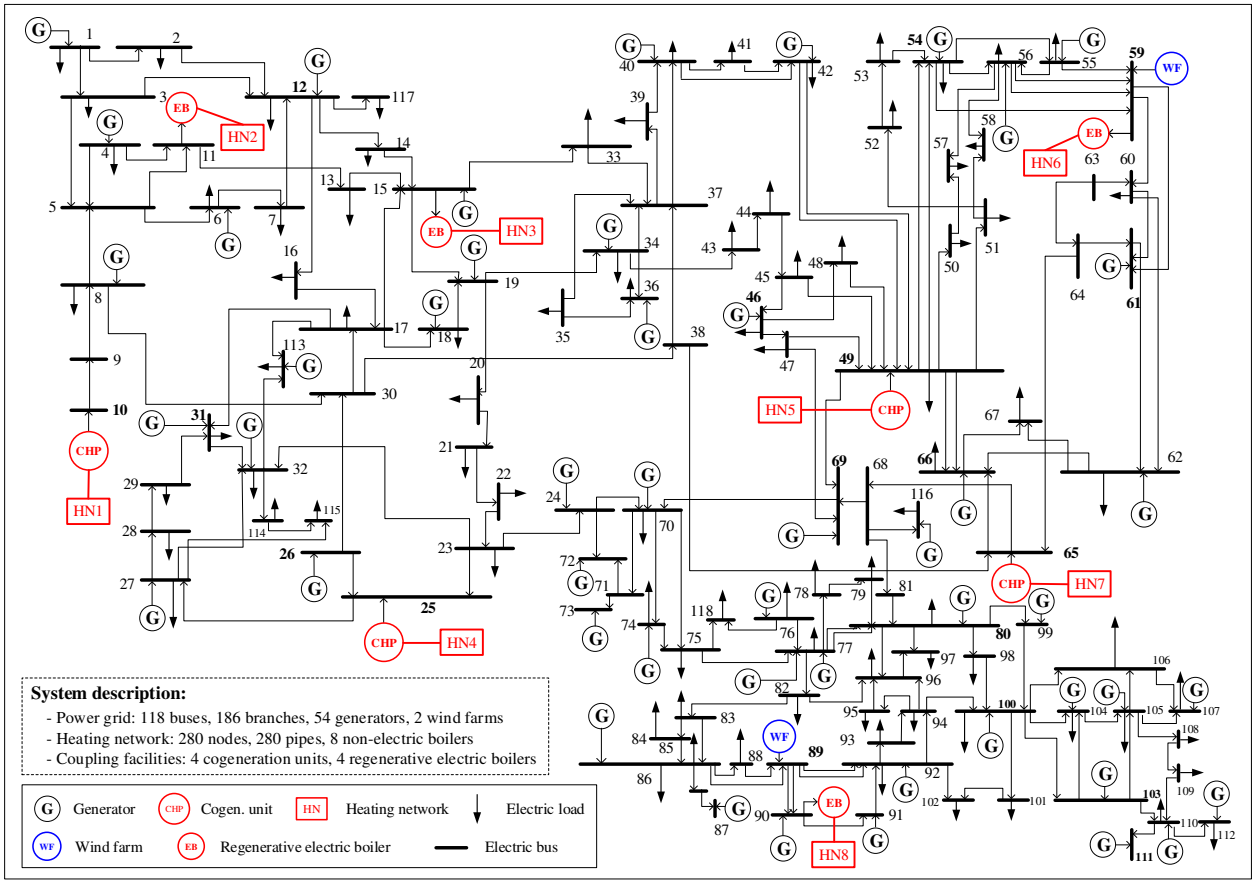

Figure 6: Schematic diagram of the test system.

5. Case Study

5.1. Test System Description

The test system consists of a modified IEEE 118-bus electric subsystem [43] and a 280-node heating subsystem, as illustrated in Figure 6. The heating subsystem is composed of eight 35-node heating subnetworks presented in [11]. The PG and 8 HNs are coupled via 4 back-pressure cogeneration units at bus 10, 25, 49, 65, and 4 regenerative electric boilers at bus 11, 15, 59 and 90. The coal-fired generator connected to bus 69 serves as the slack bus of PG.

In each HN, 3 heat sources co-supply hot water for the 21 aggregated residential loads dispersed in 5 areas [11], all operated under the quality-regulated mode. Among the 3 heat sources, Source 2 is the coupling facility linking electric and heat subsystems, while Source 1 and 3 are pure heating facilities — coal or gas boilers. More specifically, in the first heating network (denoted as HN1 in Figure 6), Source 2 is a back-pressure cogeneration unit and serves as the slack node (mT^{s} node). As for HN2 to HN8, Source 2 serves as the $m\phi$ node, while either of Source 1 or 3 serves as the slack node.

The overall simulation time is set to be 300 minutes, and the difference steps τ and h are selected as 1 minute and 90 meters for each pipe. The adjusting interval of each heat source in Stage II (τ^*) is set to be 20 minutes, and the heat loads change every 10 minutes. The fluctuating rate of electric loads and the calculation interval of power flows in PG (τ^{PG}) are both set to be 5 minutes. More details about the parameters of facilities, networks and loads can be found in [44]. Energy flow model of HN is solved by the decomposition-iteration algorithm, while that of PG is solved by MATPOWER 7.1 [45]. All tests are run in MATLAB R2021a on a computer with Intel(R) Core(TM) i7-4790 CPU @3.60 GHz and 24.0 GB memory.

5.2. Energy Flow Results of the HN

The proposed energy flow calculation method applies to all 8 heating subsystems (from HN1 to HN8) in Figure 6. As a typical example, we present and discuss the energy flow results of HN1 in this part.

First of all, part of the known conditions for energy flow analysis are given in Figure 7(a)-(c), including 1) the consumed heat power at each load node that is set to fluctuate every 10 minutes in a sinusoidal trend, as shown in Figure 7(a); 2) the heat power outputs of Source 1 and 3 that change every 20 minutes, as shown in Figure 7(b); and 3) the temperature of supply water at the adjustable-output source (i.e. Source 2) that is fixed to be 110 °C, as illustrated by the dashed purple line in Figure 7(c). Besides, the mass flow rate in each pipe and the initial temperature distribution of the HN can be found in [44].

The heat power output of Source 2 (the slack node) is illustrated by the orange line in Figure 7(b), along with the total supplied and demand heat power. When the total demand heat

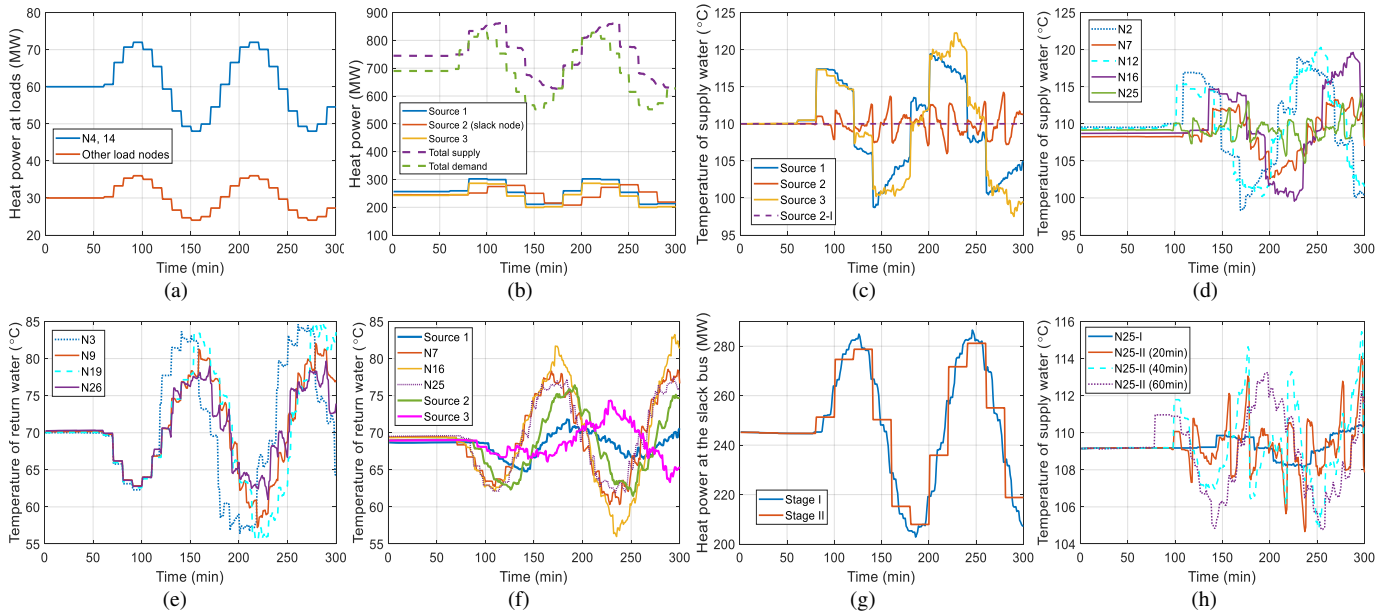

Figure 7: Energy Flow Results of the HN: (a): Consumed heat power at each load node. (b): Generated heat power at each source and system total supplied and demand heat power. (c)-(d): Temperatures of the supply water at heat sources and some intermediate nodes. (e)-(f): Temperatures of the return water at some load nodes and intermediate nodes. (g): Comparison of the heat power output of Source 2 between two stages. (h): Comparison of the supply water temperatures at N25 between two stages.

power increases or decreases, the heat power output of Source 2 will change accordingly to offset the system net power imbalance. Consequently, the temperature of return water at Source 2 will fluctuate in the opposite trends after a certain time of transmission delay, as illustrated by the dark-red line in Figure 7(f).

Further, to maintain its supply water temperatures at the set points, Source 2 will adjust its power output based on the monitored return water temperatures. This is the basic regulation rule of the slack-node source, which also accounts for the fact that the response of heat source is always one step behind the change of load, as illustrated in Figure 7(b) — the total supplied curve lags slightly behind the total demand. Besides, the mismatch between the total supplied and demand heat power is caused by the transmission heat loss and the "heat-storage" capacity of the HN.

The temperatures of supply water at two fixed-output sources are illustrated by the blue and yellow lines in Figure 7(c). The variation trends of them are co-determined by their heat power outputs and return water temperatures, as can be inferred from (A.4). Since the heat power outputs of Source 1 and 3 fluctuate in the same trend and magnitude, the variations of their supply water temperatures will be determined only by the changing trends of the return water temperatures, which are illustrated by the blue and magenta bold lines in Figure 7(f). As we can see, the return water temperatures at Source 1 and 3 share a similar variation trend in most time except for in the periods of 210-230min and 275-290min, so the blue and yellow lines in Figure 7(c) also changes in a similar trend except when they are in the above two periods. when the total supply is more than the total demand, part of the system surplus heat will be used to make up for the heat loss occurred in the delivery process, and the rest will be stored in the HN through elevating the water temperatures. By contrast, when the total supply is less than the total demand, the transmission heat loss and the deficit heat at loads will be compensated by the pre-stored heat in the HN, by means of lowering the water temperatures.

From here we see that the features of transmission delay and heat storage capacity in the HN are quite different from those in the PG, which can actually be used to accommodate the instant imbalanced electric power in the PG. Case in point, when the generated electric power far outweighs the electric demand, some of the renewable electric power can be converted into heat through electric boiler or heat pump and stored in the HN to reduce wind or solar power curtailment.

The temperatures of supply water at 5 intermediate nodes (i.e. N2, N7, N12, N16 and N25), each selected from one of the 5 load areas, are shown in Figure 7(d). The temperature profile at each one of the 5 nodes is determined, either individually or collectively, by the supply water temperatures of 3 sources. To be specific, the temperature profile at N2 is solely determined by Source 1, while that at N7 is jointly determined by Source 1 and 2, that at N12 is determined by Source 1 and 3, and those at N16 and N25 are determined by 3 Sources collectively. For N7, the variation trend of its supply water temperature is dominated by Source 1 since Source 2 fixes its temperature of supply water at 110°C. For N12, N16 and N25, the dominating source turns to be Source 3 as it is geographically closer to them. Besides, as displayed in Figure 7(d), the time delays in these temperature profiles are caused by the transmission distances away from their dominating sources. This is why the supply water temperature curve at N12 experiences the least time delay (leads all others), while the curve at N16 has the most time delay and

lags behind all. Therefore, the transmission delay of a certain node can be roughly determined as the time that it takes for the water mass to flow from its dominating source to this very node.

The temperatures of return water at some load nodes and some other intermediate nodes are displayed in Figure 7(e) and (f), respectively. Temperature profiles at load nodes are mainly affected by the variation trends of their heat power demands, and they are in fact inversely correlated — when the heat power demands rise, the temperatures of return water will fall to release more heat, and vice versa. Temperature profiles at those intermediate nodes shown in Figure 7(f) are co-determined by multiple factors, among which the temperatures of return water at some load nodes play a dominant role. The temperatures of return water at those nodes can be obtained through imposing the effects of transmission delay, heat loss and nodal fusion on the return water temperatures at their relevant load nodes. Therefore, the temperature curves at intermediate nodes share a similar variation trend with those at their relevant load nodes. From a broader view, in the whole simulation process, the temperatures of supply and return water in the HN operate near the design condition (110-70°C), as shown in Figure 7(c) to (f), which in a way shows the effectiveness of the slack source in maintaining the normal operation conditions of HN.

As discussed in Section 4.3, the heat power output at the slack node needs to be redetermined through (5) in Stage II. Comparison of the heat power outputs at Source 2 before and after modification is shown in Figure 7(g), where both curves share a similar sinusoidal variation trend. The only difference lies in that the pre-modified curve changes every 1 minute and thus appears more smooth while the modified one changes every 20 minutes. The supply water temperature curves at Source 2 in Stage I and II are comparatively presented by the dashed purple and yellow lines in Figure 7(c). Since the heat power output at Source 2 is predetermined and will remain unchanged in Stage II, its node type changes from the mT^{s} node to the $m\phi$ one, and its temperature of supply water will vary with that of the return water, instead of as being kept at 110°C in Stage I. The maximal deviation between the supply water temperatures at Source 2 in Stage I and II can reach over 4 °C.

As another example, the supply water temperatures at N25 in Stage I and II are comparatively displayed (see the blue and orange lines) in Figure 7(h) to illustrate the deviation between the energy flow results of both stages, where the results in Stage II with the adjustment interval of Source 2 being 40 and 60 minutes are also presented to see the influence of adjustment intervals on energy flow results. It can be seen that the results in Stage I and II differ significantly, and the adjustment interval has an impact on the energy flow results in Stage II. This demonstrates in a way that the modifications carried out in Stage II are necessary.

5.3. Energy Flow Results of the PG

In the power grid, electric boilers are electric loads and will serve as the *PQ* bus for energy flow analysis. The consumed active and reactive electric power at each electric boiler are respectively shown in Figure 8(a) and (b). In general, the PG is coupled with HN2, HN3, HN6 and HN8 in mode #1. It should be noted that reactive power consumptions at bus 11 and 15 are ten times magnified of its actual values in order to investigate the influence of reactive power injections on bus voltage magnitudes. The conclusions of it will be discussed later.

The cogeneration units are electric sources for the power grid and typically serve as the *PV* or slack bus for energy flow analysis. In this case, four back-pressure cogeneration units at coupling bus 10, 25, 49 and 65 are all *PV* buses, and the active electric power generations of them are displayed in Figure 8(c), where the heat-to-power ratio η^{bp} of each unit is set to be 0.6. For the cogeneration unit at bus 11, the generated electric power is determined by its heat power output since it also serves as the slack node of HN1. The PG and HN1 are coupled in mode #2. For the cogeneration units at other coupling buses, their heat and active electric power outputs are preset and will be known conditions for energy flow analysis. This means the PG is coupled with HN4, HN5 and HN7 in mode #1. The generated active electric power at bus 25, 49 and 65 are set to fluctuate sinusoidally.

To investigate the influence of operation states of HN on those of PG, we set the electric loads of PG to be time-invariant. The finally obtained electric power injections at the slack bus (bus 69) are illustrated in Figure 8(d). In general, the reactive power experiences a small level of variations while the active power fluctuates more significantly and in the opposite trends of the system net power imbalance, i.e. the difference of total demand and supply excluding the active power output of the slack-bus unit.

The bus voltage magnitudes and phase angles across the PG are more or less influenced by the operation states of HN. For those buses where the maximal difference of voltage magnitude among all simulation time points is larger than 0.003 p.u., we present their voltage magnitude variation curves in Figure 8(e) and their maximal magnitude differences in Figure 8(f). It can be seen that the voltage magnitudes at most buses experience small fluctuations except for at bus 11 and 13. This is because the bus voltage magnitude is mainly affected by reactive power flows. Since the reactive power injections at all non-*PV* buses except bus 11 and 13 vary faintly, the changing trends of the bus voltage magnitudes make sense. It should be noted that although the reactive power injections at buses 15, 59 and 90 also fluctuate significantly (As can bee seen from Figure 8(b)), the voltage magnitudes at these buses do not change because they are *PV* buses.

The phase angle variation curves at bus 9, 10, 25 and 26 are illustrated in Figure 8(g), which experience more significant fluctuations over the whole simulation process. In terms of those buses where the difference between the maximal and minimal voltage phase angles over the simulation process is larger than 13°, we illustrate the maximal phase angle differences in Figure 8(h). It can be seen that more significant changes are observed at bus 4, 5, 8, 9, 10 and 25-27 than at others, which is reasonable as the active power injections at these buses experience greater changes and the phase angles are mainly affected by the active power flows. We also observe that the active power injections at bus 49, 65 and 69 experience large fluctuations, but their phase angles do not change as much. This is because bus

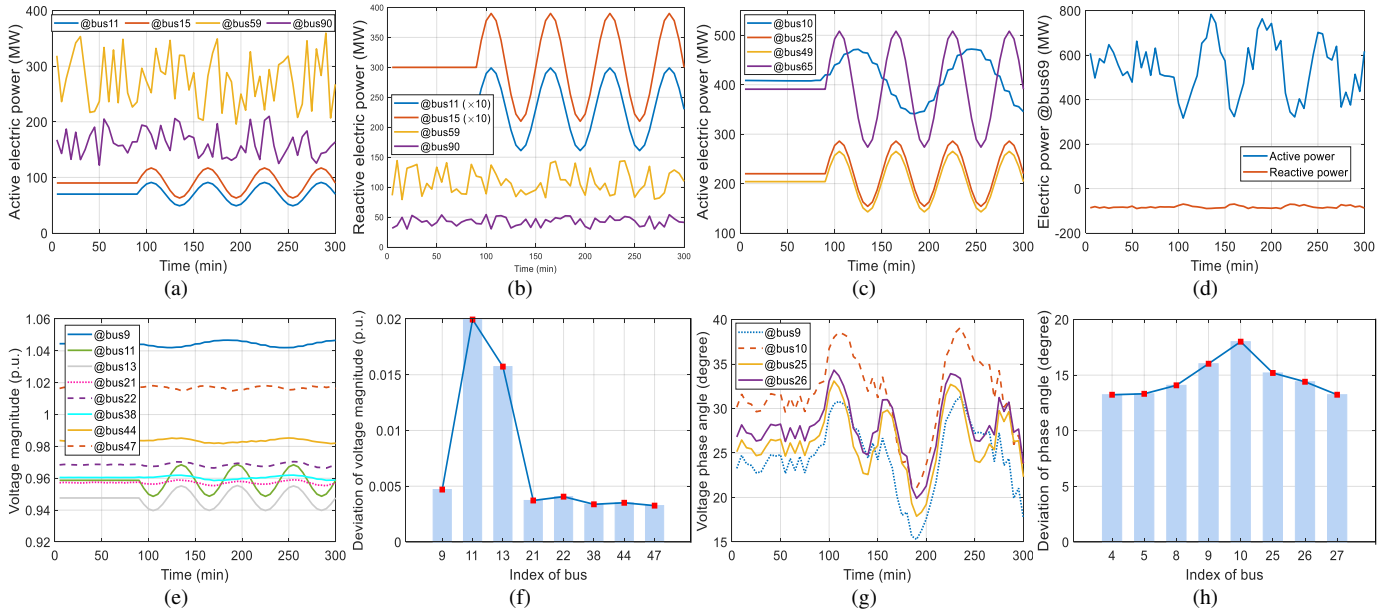

Figure 8: Energy Flow Results of the PG: (a)-(b): Consumed active and reactive electric power at bus 11, 15, 59 and 90. (c): Generated active electric power at bus 10, 25, 49 and 65. (d): Generated active and reactive electric power at the slack bus. (e): Variation curves of the voltage magnitude at some buses. (f): Maximal differences of the voltage magnitude among different time points at some buses. (g): Variation curves of the voltage phase angle at some buses. (h): Maximal differences of the voltage phase angle among different time points at some buses.

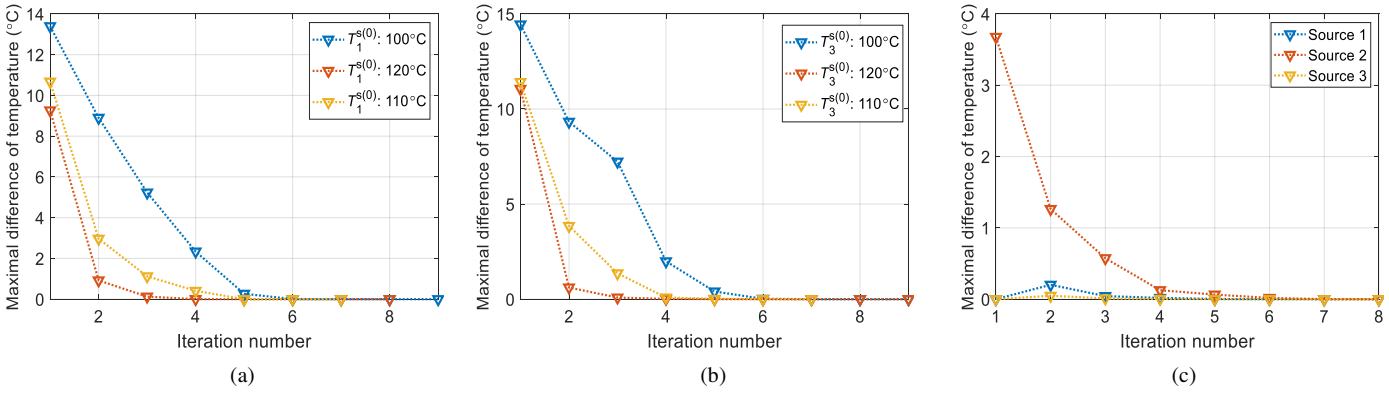

Figure 9: Convergence process of solving the energy flow models: (a)-(b): The maximal difference between the two latest updated supply water temperatures in Stage I at Source 1 and 3, respectively. (c): The maximal difference between the two latest updated supply water temperatures in Stage II at three heat sources.

69 is the slack bus with its phase angle fixed at 0°, and with its active power injections changing in the opposite trends of those at bus 49 and 65 in general. Since these three nodes are close to each other, the influence of active power injections at bus 49 and 65 are partly offset by the slack bus, and their voltage phase angles appear not to change as significantly as their active power injections do.

5.4. Convergence Processes

The convergence process of solving the energy flow model of HN in Stage I is illustrated in Figure 9(a) and (b). As has been discussed in Algorithm 1, the temperatures of supply water at all fixed-output sources (i.e. Source 1 and 3) need to be guessed beforehand and will be corrected iteratively until the difference between the two latest updated values reaches their convergence tolerance. To test the influence of initial guesses on the convergence process, we set 3 different groups of initial values (i.e. 100, 110 and 120°C) for both Source 1 and 3, and compare the updating processes of their supply water temperatures in each iteration. The convergence tolerance err_1 in this case is set to be 10^{-5}. As can be seen from Figure 7(a) and (b), for both sources, the maximal difference between the two latest updated supply water temperatures decreases to within err_1 after less than ten rounds of iteration. Although the initial guesses have some influence on the convergence rate and the number of iterations, the final energy flow results could always be efficiently obtained. The whole computing processes consumes 1.43 seconds in this stage.

The calculated supply water temperatures at heat sources in Stage I are used as the initial guess for computing the energy flow results in Stage II. The convergence tolerance err_2 in this stage is also set to be 10^{-5}, and the whole convergence pro-

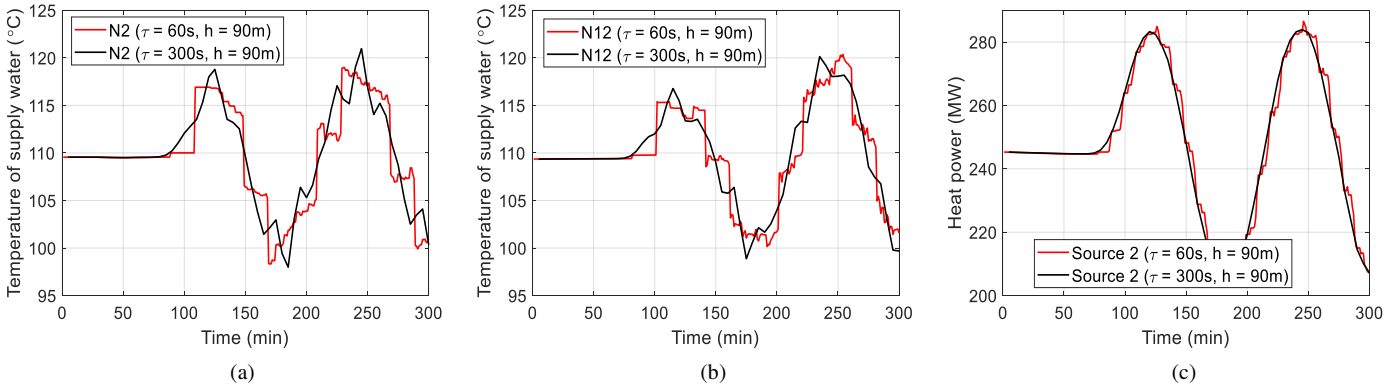

Figure 10: Comparison of energy flow results of HN in Stage I with / without matching timescales: (a)-(b): Supply water temperature curves at Node 2 and 12, respectively. (c): Heat power output at the slack source.

cess is illustrated in Figure 9(c). We can see that for all heat sources, the maximal difference between the two latest updated supply water temperatures decreases to within err_2 after about eight rounds of iteration. The whole computing process takes 1.56 seconds in this stage. In practice, the calculated supply water temperatures at all heat sources in Stage I should not differ much from the final results and therefore can simply be used as the initial values to start the iteration in Stage II.

The energy flow of PG is calculated every 5 minutes, with the built-in Newton-Raphson method in MATPOWER 7.1. It takes only 0.22 second to get the time-series energy flows of PG in this case, and at each calculation time point, convergent solutions could be obtained within 3 times of iteration. Overall, the developed method for combined energy flow analysis of the case HE-IES takes 3.21 seconds in total, which shall be qualified to provide support for system planning, operation optimization and security analysis in practical use.

5.5. Comparison of Results With / Without Matching Timescales

The proposed method for matching different timescales is in essence a sampling method that produces a set of discrete data points from another set of discrete data points with a different sequence interval. If the step of matching timescales is left out, the energy flows of HN and PG need to be calculated with the same interval.

For the case study in Section 5, if the calculation interval of HN (1 minute) is adopted for both PG and HN, the obtained energy flow results with / without the proposed strategy are the same, but the calculation rounds of power flow in the PG are fivefold since the calculation interval for PG changes from 1minute to 5 minutes, and the total computation time increases from 3.21 seconds to 4.05 seconds.

Alternatively, if the calculation interval of PG (5 minute) is adopted for both PG and HN, considerable errors might occur in the obtained energy flow results of HN. For example, in our case study, the comparisons of the supply water temperature curves at Node 2 and 12 with / without timescale match in Stage I are displayed in Figure 10(a) and (b), where larger calculation interval obviously omits more temperature variation details and causes certain errors. The maximal temperature deviation for Node 2 reaches 5.9°C (5.5%), while that for Node 12 is 4.1°C (4.0%). The comparison of heat power output at the slack source in Stage I is shown in Figure 10(c), where the maximal heat power deviation hits 9.2MW (3.8%).

Therefore, the proposed strategy of matching timescales can either help reduce the overall computation workload or improve the accuracy of energy flow results.

5.6. Further Discussion

This part presents some more physical explanations of the simulation results and extends them into more general situations, aiming to provide some generic and instructive advice in practical applications.

First, it can be seen from Figure 7(h) that the larger the adjusting interval of heat sources in Stage II differs from the temporal step size of HN, the larger error can be caused in the calculated energy flow results. In practical heating networks, the temporal step size is usually several minutes, while the adjusting interval of heat sources can be several tens of minutes. Therefore, it is necessary to introduce Stage II to modify the inaccurate energy flow results in most practical systems.

Second, Figure 7(e) - (h) show that the influence of HN on PG is mainly imposed by changing the injected electric power of the coupling facilities, which further influences the voltage magnitudes and phase angles of the whole PG. Further, those buses that are adjacent to the coupling facilities tend to be affected more significantly, so more attention are ought be paid to them in the security check process of practical power grids.

Third, the convergence performance shown in Figure 9(a) and (b) indicates that the selected initial values do not have essential influence on the convergence process. Therefore, in practical HNs the design supply water temperature is recommended as the initial values of the supply water temperatures at all fixed-output sources in Stage I for simplicity.

Finally, the results illustrated in Figure 10 also partly show the influence of temporal difference step size τ on the energy flow results. Generally, different step sizes can cause certain degree of errors that may not be neglected. Since the computing error is proportional to the square of τ, it is recommended to

use as small step size as possible to calculate the energy flows of HN on the premise of meeting the solution time limits.

6. Conclusion

This paper presents a systematic study on combined dynamic energy flow analysis of PG and HN. The quasi-dynamic HN model described by PDEs is adopted to capture the long-lasting temperature dynamics in the pipeline. Starting from a thorough coupling analysis of PG and HN, the decoupling method for combined energy flow analysis in each coupling mode is developed, where a data processing method is also proposed to settle the timescale mismatches occurred in the interactions between PG and HN.

On this basis, a refined difference scheme is employed to discretize the PDEs into high-dimensional AEs, which are then efficiently solved by a novel decomposition-iteration algorithm. Compared with existing methods, this algorithm avoids deriving the gigantic coefficient matrix of network equations and can yield more accurate energy flow results. The convergence of this algorithm is also analyzed analytically and numerically.

Finally, to eliminate the systematical error caused by leaving out the inertial and adjusting constraints of heat sources, a revision stage is firstly introduced to modify the calculated energy flow results, which helps to obtain closer-to-reality state information. Results in the case study demonstrate the effectiveness and efficiency of the proposed methods.

7. Future work

Generally, larger temporal and spatial difference steps will cause larger errors, which means on the premise of satisfying the computation time limits, selecting as small difference steps as possible helps improve the simulation accuracy. However, to what extent will the accuracy of the energy flow results be affected by different steps on different heating networks and how to select an optimal combination of temporal and spatial difference steps to achieve the best compromise between simulation workload and model accuracy still require both theoretical analysis and massive numerical experiments on different scales of test systems, which is one of our future research focuses.

Also, the proposed decomposition-iteration algorithm iteratively solves the models of supply water network, heat loads, return water network and heat sources to output the final convergent energy flows of HN. If the four entities can be modeled as a whole, a non-iterative algorithm may be hopefully employed to further reduce the computation burden and remove the reliance on initial variable guesses, which will be cared about in our future work.

Lastly, the proposed energy flow analysis methods in this paper only apply to the IES with PG and quality-regulated HN. Developing the combined energy flow analysis methods of the IES with quantity-regulated hot-water HN and with steam HN is our further research concerns.

CRediT Authorship Contribution Statement

Shuai Yao: Ideas, Modeling, Methods, Software & Validation. **Wei Gu**: Ideas, Methods, Review & Editing. **Jianzhong Wu**: Ideas, Methods & Revision. **Hai Lu**: Resources & Modeling. **Suhan Zhang**: Methods & Revision. **Yue Zhou**: Methods, Review & Editing. **Shuai Lu**: Methods & Revision.

Declaration of Competing Interest

The authors declare that they have no known competing financial interests or personal relationships that could have appeared to influence the work reported in this paper.

Acknowledgment

This work is Supported by the National key Research and Development Program of China (Grant No. 2020YFE0200400), the Smart Grid Joint Fund of National Science Foundation of China & State Grid Corporation of China (Grant No. U1866208), the Scientific Research Foundation of Graduate School of Southeast University (Grant No. YBPY2152) and the Chinese Scholarship Council.

We also deeply appreciate the support received from the Engineering and Physical Sciences Research Council (EPSRC) through the project "Integrated heating and cooling networks with heat-sharing-enabled smart prosumers" (EP/T022795/1).

AppendixA. Equations Used in Algorithm 1

$$\begin{cases} T_{j,i}^{k+1} = \varpi_{1,j} \cdot T_{j,i-1}^{k} + \varpi_{2,j} \cdot T_{j,i-1}^{k+1} + \varpi_{3,j} \cdot T_{j,i}^{k} + \varpi_{4,j} \cdot T^{\mathrm{a},k} \\ \qquad (i = 1, 2, \cdots M_j;\ k = 0, 1, \cdots, N_j - 1;\ \forall j \in \mathbb{E}^{\mathrm{s}}) \\ \sum_j (\dot{m}_{n,j}^{\mathrm{in}} \cdot T_{n,j}^{\mathrm{in}}) = T_n \cdot \sum_j \dot{m}_{n,j}^{\mathrm{in}} \quad \forall n \in \mathbb{V}^{\mathrm{si}},\ j \in \mathbb{E}_n^{\mathrm{si,in}} \\ T_{n,j}^{\mathrm{out}} = T_n \qquad \forall n \in \mathbb{V}^{\mathrm{si}},\ j \in \mathbb{E}_n^{\mathrm{si,out}} \end{cases} \tag{A.1}$$

$$T_j^{\mathrm{r}} = T_j^{\mathrm{s}} - \phi_j / c / \dot{m}_j \qquad \forall j \in \mathbb{V}^{\mathrm{l}} \tag{A.2}$$

$$\begin{cases} T_{j,i}^{k+1} = \varpi_{1,j} \cdot T_{j,i-1}^{k} + \varpi_{2,j} \cdot T_{j,i-1}^{k+1} + \varpi_{3,j} \cdot T_{j,i}^{k} + \varpi_{4,j} \cdot T^{\mathrm{a},k} \\ \qquad (i = 1, 2, \cdots M_j;\ k = 0, 1, \cdots, N_j - 1;\ \forall j \in \mathbb{E}^{\mathrm{r}}) \\ \sum_j (\dot{m}_{n,j}^{\mathrm{in}} \cdot T_{n,j}^{\mathrm{in}}) = T_n \cdot \sum_j \dot{m}_{n,j}^{\mathrm{in}} \quad \forall n \in \mathbb{V}^{\mathrm{ri}},\ j \in \mathbb{E}_n^{\mathrm{ri,in}} \\ T_{n,j}^{\mathrm{out}} = T_n \qquad \forall n \in \mathbb{V}^{\mathrm{ri}},\ j \in \mathbb{E}_n^{\mathrm{ri,out}} \end{cases} \tag{A.3}$$

$$T_j^{\mathrm{s}} = T_j^{\mathrm{r}} + \phi_j / c / \dot{m}_j \qquad \forall j \in \mathbb{V}^{\text{s-f}} \tag{A.4}$$

$$T_j^{\mathrm{s}} = T_j^{\mathrm{r}} + \phi_j / c / \dot{m}_j \qquad \forall j \in \mathbb{V}^{\mathrm{s}} \tag{A.5}$$

Reference

[1] Wu J, Yan J, Jia H, Hatziargyriou N, Djilali N, Sun H. Integrated energy systems. Applied Energy 2016;167:155 –7. doi:10.1016/j.apenergy.2016.02.075.

[2] Berjawi A, Walker S, Patsios C, Hosseini S. An evaluation framework for future integrated energy systems: A whole energy systems approach. Renewable and Sustainable Energy Reviews 2021;145:111163. doi:10.1016/j.rser.2021.111163.

[3] Yan M, Gan W, Zhou Y, Wen J, Yao W. Projection method for blockchain-enabled non-iterative decentralized management in integrated natural gas-electric systems and its application in digital twin modelling. Applied Energy 2022;311:118645. doi:h10.1016/j.apenergy.2022.118645.

[4] Zhang X, Strbac G, Shah N, Teng F, Pudjianto D. Whole-system assessment of the benefits of integrated electricity and heat system. IEEE Transactions on Smart Grid 2019;10(1):1132–45. doi:10.1109/TSG.2018.2871559.

[5] Chen X, Kang C, O'Malley M, Xia Q, Bai J, Liu C, et al. Increasing the flexibility of combined heat and power for wind power integration in china: modeling and implications. IEEE Transactions on Power Systems 2015;30(4):1848–57. doi:10.1109/TPWRS.2014.2356723.

[6] Gu W, Wang J, Lu S, Luo Z, Wu C. Optimal operation for integrated energy system considering thermal inertia of district heating network and buildings. Applied Energy 2017;199:234 –46. doi:https://doi.org/10.1016/j.apenergy.2017.05.004.

[7] Yao S, Gu W, Zhou S, Lu S, Wu C, Pan G. Hybrid timescale dispatch hierarchy for combined heat and power system considering the thermal inertia of heat sector. IEEE Access 2018;6:63033–44. doi:10.1109/ACCESS.2018.2876718.

[8] Lu S, Gu W, Meng K, Yao S, Liu B, Dong ZY. Thermal inertial aggregation model for integrated energy systems. IEEE Transactions on Power Systems 2020;35(3):2374–87. doi:10.1109/TPWRS.2019.2951719.

[9] Yan J, He H, Sun Y. Integrated security analysis on cascading failure in complex networks. IEEE Transactions on Information Forensics and Security 2014;9(3):451–63. doi:10.1109/TIFS.2014.2299404.

[10] Pan Z, Wu J, Sun H, Guo Q, Abeysekera M. Quasi-dynamic interactions and security control of integrated electricity and heating systems in normal operations. CSEE Journal of Power and Energy Systems 2019;5(1):120–9. doi:10.17775/CSEEJPES.2018.00240.

[11] Liu X, Wu J, Nick J, Audrius B. Combined analysis of electricity and heat networks. Applied Energy 2016;162:1238 –50. doi:https://doi.org/10.1016/j.apenergy.2015.01.102.

[12] Qin X, Sun H, Shen X, Guo Y, Guo Q, Xia T. A generalized quasi-dynamic model for electric-heat coupling integrated energy system with distributed energy resources. Applied Energy 2019;251:113270. doi:10.1016/j.apenergy.2019.05.073.

[13] Pan Z, Guo Q, Sun H. Interactions of district electricity and heating systems considering time-scale characteristics based on quasi-steady multi-energy flow. Applied Energy 2016;167:230–43. doi:10.1016/j.apenergy.2015.10.095.

[14] Li J, Huang Y, Zhu M. Gradient descent iterative method for energy flow of integrated energy system considering multiple modes of compressors. Energy Conversion and Management 2020;207(100):112534. doi:10.1016/j.enconman.2020.112534.

[15] Chen D, Hu X, Li Y, Wang R, Abbas Z, Zeng S, et al. Nodal-pressure-based heating flow model for analyzing heating networks in integrated energy systems. Energy Conversion and Management 2020;206:112491. doi:10.1016/j.enconman.2020.112491.

[16] Wang L, Zheng J, Li M, Lin X, Jing Z, Wu P, et al. Multi-time scale dynamic analysis of integrated energy systems: An individual-based model. Applied Energy 2019;237:848–61. doi:10.1016/j.apenergy.2019.01.045.

[17] Shabanpour-Haghighi A, Seifi AR. An integrated steady-state operation assessment of electrical, natural gas, and district heating networks. IEEE Transactions on Power Systems 2016;31(5):3636–47. doi:10.1109/TPWRS.2015.2486819.

[18] Ayele GT, Haurant P, Laumert B, Lacarrière B. An extended energy hub approach for load flow analysis of highly coupled district energy networks: Illustration with electricity and heating. Applied Energy 2018;212:850–67. doi:10.1016/j.apenergy.2017.12.090.

[19] Shi J, Wang L, Wang Y, Zhang J. Generalized energy flow analysis considering electricity gas and heat subsystems in local-area energy systems integration. Energies 2017;10(4):1–17. doi:10.3390/en10040514.

[20] Qu L, Ouyang B, Yuan Z, Zeng R. Steady-state power flow analysis of cold-thermal-electric integrated energy system based on unified power flow model. Energies 2019;12(23). doi:10.3390/en12234455.

[21] Zhang G, Zhang F, Meng K, Zhang X, Dong Z. A fixed-point based distributed method for energy flow calculation in multi-energy systems. IEEE Transactions on Sustainable Energy 2020;11(4):2567–80. doi:10.1109/TSTE.2020.2966737.

[22] Sun Q, Dong Q, You S, Li Z, Wang R. A unified energy flow analysis considering initial guesses in complex multi-energy carrier systems. Energy 2020;213:118812. doi:10.1016/j.energy.2020.118812.

[23] Massrur H, Niknam T, Aghaei J, Shafie M, Catalao J. Fast decomposed energy flow in large-scale integrated electricity-gas-heat energy systems. IEEE Transactions on Sustainable Energy 2018;9(4):1565–77. doi:10.1109/TSTE.2018.2795755.

[24] Sun G, Wang W, Lu X, Wu Y, Hu W, Yang Z, et al. Rapid energy flow calculation method for integrated electrical and thermal systems. International Journal of Electrical Power & Energy Systems 2020;123(July 2019). doi:10.1016/j.ijepes.2020.106317.

[25] Gao P, Zhou X, Yang X, Li Y. Sequence iterative method-based steady-state analysis of integrated electricity, gas and heating networks. International Journal of Electrical Power & Energy Systems 2021;124(July 2020):106359. doi:10.1016/j.ijepes.2020.106359.

[26] Dancker J, Wolter M. Improved quasi-steady-state power flow calculation for district heating systems: A coupled newton-raphson approach. Applied Energy 2021;295:116930. URL: 10.1016/j.apenergy.2021.116930. doi:10.1016/j.apenergy.2021.116930.

[27] Chenand H. Sun B, Wu W, Guo Q, Qiao Z. Energy circuit theory of integrated energy system analysis (iii): steady and dynamic energy flow calculation. Proceedings of the Chinese Society of Electrical Engineering 2020;40(15):4820–31. doi:https://10.13334/j.0258-8013.pcsee.200647.

[28] Yang J, Zhang N, Sun H. Analysis theory of generalized electric circuit for multi-energy networks – part two network model. Automation of Electric Power Systems 2020;44(10). doi:https://10.7500/AEPS20200209002.

[29] Benonysson A. Dynamic modeling and operational optimization of district heating system. Ph.D. thesis; Tech. Uni. Denmark; Lyngby; 1991.

[30] Li Z, Wu W, Shahidehpour M, Wang J, Zhang B. Combined heat and power dispatch considering pipeline energy storage of district heating network. IEEE Transactions on Sustainable Energy 2016;7(1):12–22. doi:10.1109/TSTE.2015.2467383.

[31] Lu S, Gu W, Zhang C, Meng K, Dong Z. Hydraulic-thermal cooperative optimization of integrated energy systems: a convex optimization approach. IEEE Transactions on Smart Grid 2020;11(6):4818–32. doi:10.1109/TSG.2020.3003399.

[32] Stevanovic VD, Zivkovic B, Prica S, Maslovaric B, Karamarkovic V, Trkulja V. Prediction of thermal transients in district heating systems. Energy Conversion Management 2009;50(9):2167–73.

[33] David MY. Iterative solution of large linear systems. New York: Academic Press; 1971. ISBN 978-0-12-773050-9. doi:https://doi.org/10.1016/B978-0-12-773050-9.50009-7.

[34] Yang J, Zhang N, Botterud A, Kang C. On an equivalent representation of the dynamics in district heating networks for combined electricity-heat operation. IEEE Transactions on Power Systems 2020;35(1):560–70. doi:10.1109/TPWRS.2019.2935748.

[35] Yao S, Gu W, Lu S, Zhou S, Wu Z, Pan G, et al. Dynamic optimal energy flow in the heat and electricity integrated energy system. IEEE Transactions on Sustainable Energy 2021;12(1):179–90. doi:10.1109/TSTE.2020.2988682.

[36] Wang Y. Research on dynamic characteristic analysis and robust optimal control of district heating system. Ph.D. thesis; Tianjin University; 2017. URL: https://kns.cnki.net/KCMS/detail/detail.aspx?dbname=CMFD201901&filename=1018894458.nh.

[37] Zimmerman RD, Murillo-Sánchez CE. Matpower user's manual 7.1. 2020. doi:10.5281/zenodo.4074122.

[38] CHPQA . The CHPQA Standard. 2016. URL: https://assets.publishing.service.gov.uk/government/uploads/system/uploads/attachment_data/file/569406/

CHPQAStandardIssue6.pdf.

[39] CHPQA . GUIDANCE NOTE 28: the determination of Z ratio. 2007. URL: https://www.chpqa.com/guidance_notes/GUIDANCE_NOTE_28.pdf.

[40] Fang J, Zeng Q, Ai X, Chen Z, Wen J. Dynamic optimal energy flow in the integrated natural gas and electrical power systems. IEEE Transactions on Sustainable Energy 2018;9(1):188–98. doi:10.1109/TSTE.2017.2717600.

[41] Thomas J. Numerical partial differential equations: finite difference methods. New York: Springer Science+Business Media; 1995. ISBN 978-1-4419-3105-4. doi:https://doi.org/10.1007/978-1-4899-7278-1.

[42] Yao S. Convergence analysis of the decomposition-iteration algorithm. 2022. URL: https://dx.doi.org/10.21227/h2mz-0g54. doi:10.21227/h2mz-0g54.

[43] Zimmerman RD, Murillo-Sánchez CE, Thomas RJ. Matpower: Steady-state operations, planning, and analysis tools for power systems research and education. IEEE Transactions on Power Systems 2011;26(1):12–9. doi:10.1109/TPWRS.2010.2051168.

[44] Yao S. Data of the coupled 118-bus power system and 280-node heating system. 2022. doi:10.21227/trz0-5434.

[45] Zimmerman RD, Murillo-Sánchez CE. Matpower 7.1. 2020. doi:10.5281/zenodo.4074135.